

# Crystallochemical Characterizations, Raman Spectroscopy and Studies Nuclear Magnetic Resonance (NMR) of $\text{Cu}_2\text{Zn}(\text{Sn}, \text{Si})\text{S}_4$ Compounds for Photovoltaic Applications

Mohamed Hamdi<sup>1</sup>, Messaoud Benamira<sup>2</sup>

<sup>1</sup>Northern Border University, Arar, Turaif, Saudi Arabia

<sup>2</sup>Laboratory of Interaction Materials and Environment (LIME), University of Mohamed Seddik Ben Yahia-Jijel, Jijel, Algeria  
Email: hamdymed@gmail.com

**How to cite this paper:** Hamdi, M. and Benamira, M. (2022) Crystallochemical Characterizations, Raman Spectroscopy and Studies Nuclear Magnetic Resonance (NMR) of  $\text{Cu}_2\text{Zn}(\text{Sn}, \text{Si})\text{S}_4$  Compounds for Photovoltaic Applications. *Journal of Materials Science and Chemical Engineering*, 10, 24-40.

<https://doi.org/10.4236/msce.2022.101002>

**Received:** November 22, 2021

**Accepted:** January 21, 2022

**Published:** January 24, 2022

Copyright © 2022 by author(s) and Scientific Research Publishing Inc. This work is licensed under the Creative Commons Attribution International License (CC BY 4.0).

<http://creativecommons.org/licenses/by/4.0/>



Open Access

## Abstract

In this study, Si-doped  $\text{Cu}_2\text{ZnSnS}_4$  compounds ( $\text{Cu}_2\text{ZnSn}_{1-x}\text{Si}_x\text{S}_4$ ,  $0 \leq x \leq 1$ ) were prepared by solid state reaction method for use of materials for photovoltaic cells. The structural and spectroscopic properties of the as-prepared compounds were studied by X-ray diffraction (XRD),  $^{119}\text{Sn}$ ,  $^{29}\text{Si}$  and  $^{65}\text{Cu}$  Magic Angle Spinning nuclear magnetic resonance (MAS NMR) and Raman spectroscopy. The Si-substitution in the Sn-site induces three different types of XRD patterns which depend largely on the Si content in the compound. For  $0 \leq x \leq 0.5$ , XRD analysis reveals the presence of a pure tetragonal phase of solid solution with I-42m as a space group. Mixed tetragonal and orthorhombic phases were observed for  $0.5 < x < 0.8$ , followed by a pure orthorhombic structure with a space group Pmn2<sub>1</sub> at high content of Si ( $x \geq 0.8$ ).  $^{119}\text{Sn}$  MAS NMR spectra show the presence of Sn/Si disorder as a function of the Si content. The  $^{65}\text{Cu}$  MAS NMR spectra of the quadratic solid solution confirm the presence of the two copper sites (Cu-2a and Cu-2c) at 780 ppm while in the case of the orthorhombic solid solution samples, a very broad band is observed. The optical properties were investigated of all compounds by UV-Vis diffuse reflectance and the obtained optical band gap values (1.31 to 2.43 eV) confirm a semiconductor character.

## Keywords

Photovoltaic Cells,  $\text{Cu}_2\text{ZnSnS}_4$ , Nuclear Magnetic Resonance, Raman Spectroscopy

## 1. Introduction

Nowadays, the use of clean energy resources such as solar energy becomes one of the relevant challenges of researchers in order to limit the damage caused by the use of fossil energy. The use of solar cells as a source of electricity generation has been increasing in the last decade due to the decrease in the cost of the fabrication materials and the increase in efficiency. The manufacture of solar cells based on non-toxic and abundant materials is a major challenge for the development of renewable energies in general, and photovoltaic applications in particular. One of the most promising ways is the use of thin layers of semiconductor materials based on the compound  $\text{Cu}_2\text{ZnSnS}_4$  (CZTS) as a light absorber instead of  $\text{Cu}(\text{In}, \text{Ga})(\text{S}, \text{Se})_2$  alloys which contain chemical elements with a limited availability [1]-[7]. Its use is associated with the presence of local disorder which can be beneficial for high performance. CZTS semiconductor compound greater than 30% [8] and an energy band gap ( $E_g$ ) value which varies between 1.4 and 1.7 eV depend on the method used to determine  $E_g$  value from the UV-Vis diffuse reflectance spectra and also the preparation condition of this material [9] [10] [11]. Malerba *et al.* prepared CZTS thin films using sulfurization method with different compositions of the initial precursors of ZnS, Cu and Sn. The obtained band gap values, between 1.48 and 1.63 eV, are influenced by the increase of the  $[\text{Sn}]/[\text{Cu}]$  ratio responsible for the formation of additional defects [12]-[17].

Nitsche *et al.* report the first study about the synthesis of CZTS compound using iodine vapor transport method [18]. Different attempt was conducted to synthesize CZTS thin layers using several methods such as thermal evaporation, atomic layer deposition, sol gel, radio frequency magnetron sputtering and spray method [19] [20] [21] [22] [23].

In this study, we investigate the effect of the partial chemical substitution of Sn by Si in  $\text{Cu}_2\text{ZnSnS}_4$  semiconductor on the structural, spectroscopic and optical properties. Our main objective is to expand the family of these quaternary chalcogenides (CZTS) by gradually replacing tin with silicon ( $\text{Cu}_2\text{ZnSn}_{1-x}\text{Si}_x\text{S}_4$ ,  $0 \leq x \leq 1$ ). The substitution of Sn by Si leads to a decrease in lattice volume due to the difference in atomic radii between Sn and Si. Moreover, the two limit compounds of this series have two different crystal structures,  $\text{Cu}_2\text{ZnSnS}_4$  with tetragonal phase and  $\text{Cu}_2\text{ZnSiS}_4$  with orthorhombic phase.

## 2. Experimental Section

Synthesis and chemical analyses: the synthesis route was adapted from the one proposed by L. Choubrac *et al.* [24]. Namely, the compounds were prepared at  $900^\circ\text{C}$  by solid state reactions from elemental Cu, Zn, Sn, Si, S precursors weighted in the appropriate ratios respectively 2:1:1-x:x:4 in dry box for 1 week. The reagents were weighted in stoichiometric ratio and put together into a fused silica tube. The tube was flame sealed under vacuum, heated to  $900^\circ\text{C}$  (with intermediate temperature steps at  $250^\circ\text{C}$  and  $450^\circ\text{C}$  for two hours) and held at that

temperature for 1 week. The as-obtained samples were then ground in an agate mortar and annealed at the synthesis temperature for 96 h to improve the homogeneity and the crystallization of the powders, then subsequently quenched in an iced bath [25]. At this stage, X-ray powder diffraction analyses did not detect any sub-products.

The elemental composition of the studied samples is a critical point for this study, and many efforts were made to ensure both accuracy and precision in these measurements. Practically, powders were embedded in epoxy and polished to get a perfect flat surface of the grains. Additionally, the systematic use of standards (Cu, Zn, Sn, CaSiO<sub>3</sub>, FeS<sub>2</sub>) ensures that the obtained chemical compositions are both precise and accurate. Because the silicon weight percentage remains low in most of the studied compounds, the atomic silicon content is not very accurate.

### 3. Results and Discussion

#### 3.1. Structural Analysis

The XRD patterns of Cu<sub>2</sub>Zn(Sn<sub>1-x</sub>Si<sub>x</sub>)S<sub>4</sub> (0 ≤ x ≤ 1) were obtained after calcination. The Si-substitution of Cu<sub>2</sub>ZnSnS<sub>4</sub> in the Sn-site induces three different types of XRD patterns which depend largely on the content of Si in the compound [25]. For 0 ≤ x ≤ 0.5, XRD analysis reveals the presence of pure phase of solid solution in which the peak positions shift for more positive values of  $\theta$  while Si content increases in the kesterite structure. This is related with the difference in atomic radii between Sn and Si ( $r_{\text{Sn}}$  (1.62 Å) >  $r_{\text{Si}}$  (1.32 Å)) [25]. All XRD diffraction maxima can be indexed in a tetragonal phase with I-42m space group. The lattice parameters were obtained using Le Bail refinement in Fullprof software, the results are regrouped in **Table 1**. The associated lattice parameters decrease with the increase of Si content which can be attributed to the low atomic radii of Si compared to Sn. The study of the evolution of the lattice parameters of the tetragonal structure as a function of the Si content indicates a linear fit and follows Vegard's law [26] (**Figure 1**). It should be noted that the variation in lattice parameters is less than 2%.

In the case of 0.5 < x < 0.8, XRD patterns reveal the presence of diffraction maxima attributed to tetragonal phase and also the presence of new diffraction maxima attributed to the orthorhombic structure with space group Pmn2<sub>1</sub>. Moreover, the lattice parameters are practically unchanged with the Si content in this region which is a typical signature of a two-phase domain between two solid solutions transition. However, while x is ≥ 0.8, All XRD diffraction maxima are indexed with the pure and single orthorhombic phase. The lattice parameters of Cu<sub>2</sub>ZnSiS<sub>4</sub> (x = 1.0) obtained in this study are in accordance with those reported in the literature [27]. This study confirms that Cu<sub>2</sub>Zn(Sn<sub>1-x</sub>Si<sub>x</sub>)S<sub>4</sub> compounds present pure tetragonal phase for low content of Si (x ≤ 0.5), the increase of Si content is associated with the formation of an additional orthorhombic phase before the transition phase observed for x = 0.8 and the formation of single and pure orthorhombic phase.

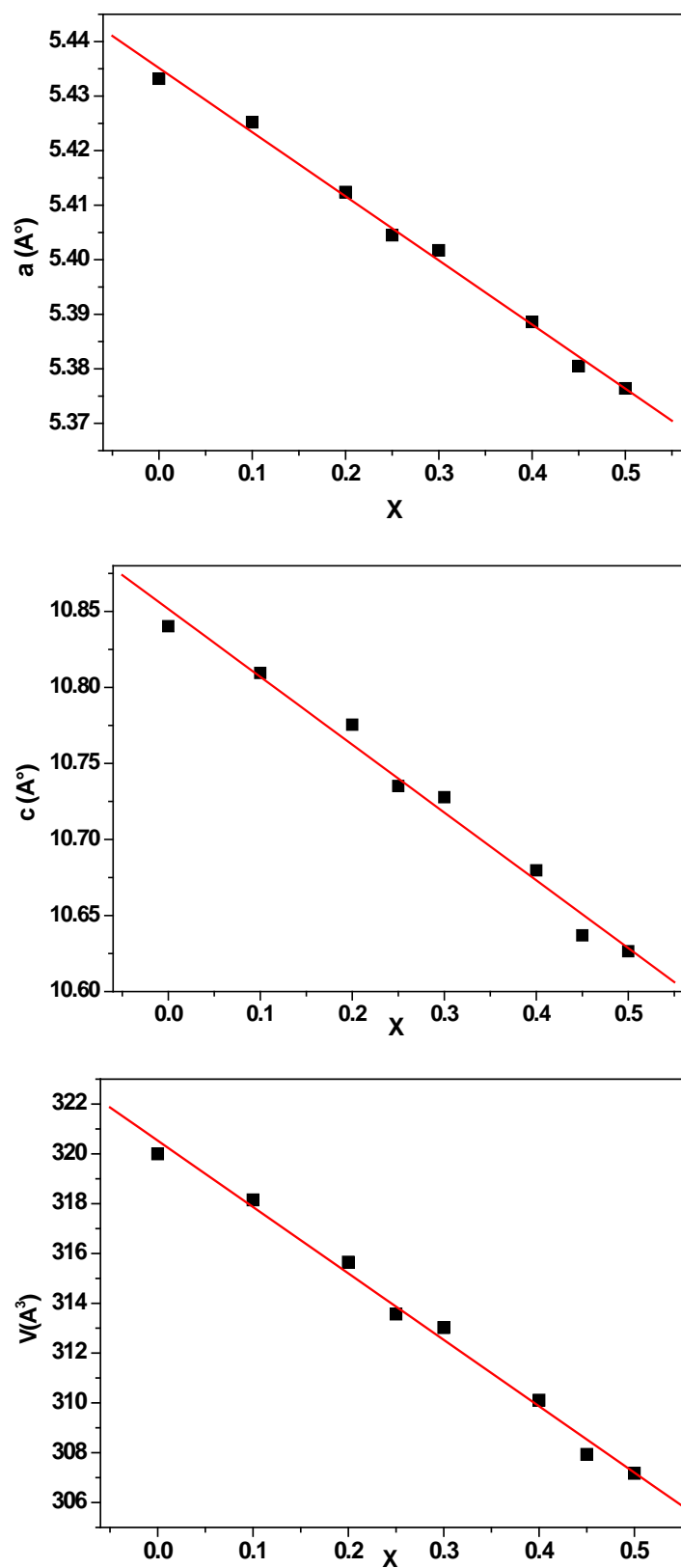


**Figure 1.** Variation of lattice parameters ( $a$ ,  $c$  and volume  $v$ ) as a function of the silicon content in the solid solution ( $0 \leq x \leq 0.5$ ). The Si content is deduced from the measured volume and the equation of Vegard's law.

**Table 1.** Tetragonal unit cell parameters evolution versus the targeted Si-content,  $x = \text{Si}/(\text{Sn}/\text{Si})$ , in the  $\text{Cu}_2\text{Zn}(\text{Sn}, \text{Si})\text{S}_4$  series from the PXRD investigation.

Samples	phases	a (Å)	b (Å)	c (Å)	V (Å <sup>3</sup> )
Si00-21	T	5.4332(2)		10.8402(6)	320.00(5)
Si10-11	T	5.4252(1)		10.8095(2)	318.15(2)
Si20-11	T	5.4124(2)		10.7755(6)	315.65(4)
Si25-11	T	5.4045(1)		10.7352(2)	313.57(1)
Si30-11	T	5.4017(2)		10.7278(5)	313.02(3)
Si40-31	T	5.3886(1)		10.6797(4)	310.11(3)
Si45-21	T	5.3805(5)		10.369(16)	307.93(10)
Si50-41	T	5.3764(4)		10.6265(9)	307.17(8)
Si60-11	T	5.3747(3)		10.6184(3)	306.74(5)
	O	7.4729(5)	6.4341(4)	6.1743(5)	296.87(6)
Si75-11	T	5.3756(2)		10.6168(6)	306.79(4)
	O	7.4800(3)	6.4394(3)	6.1662(3)	297.02(4)
Si80-11	O	7.4862(1)	6.4501(1)	6.1769(1)	298.27(1)
Si100-11	O	7.4372(2)	6.3986(2)	6.1381(1)	292.11(2)

### 3.2. Raman Analysis of $\text{Cu}_2\text{Zn}(\text{Sn}_{1-x}\text{Si}_x)\text{S}_4$ Compounds

In order to correlate properties with structure, Raman analysis was conducted. According to the literature, stoichiometric CZTS compounds with kesterite structure have 27 optically active modes [28] [29]. Optimization of measurement conditions by choosing the appropriate equipment, power, laser, acquisition time, powder or crystal sample were the first step of this study. Preliminary measurements made on the visible dispersive Raman of the “Jobin-Yvon T64000” type, containing a CCD detector cooled by liquid nitrogen, require long counting times that are not always compatible with the need to carry out a large number of measurements. Visible Raman assembly dedicated to mapping “Renishaw In Via reflex” was used and the detection is optimized for short counting times (a few seconds). All measurements were done with green excitation (514.5 nm laser), 0.15 mW power and an acquisition time of 30 seconds.

Recently, Caballero *et al.* [30] suggested that the structural disorder, due to deviations from the stoichiometry or to the copper/zinc disorder which increases the width of the peaks, is the origin of a characteristic peak around  $332 \text{ cm}^{-1}$  and the peak at  $338 \text{ cm}^{-1}$  is the signature of the ordered kesterite structure.

**Figure 2** shows the Raman spectra of the sample Si00 with rapid cooling (quenching, Si00-21) and slow cooling (Si00-31) with a rate of  $20^\circ\text{C}/\text{h}$ . The width of the majority of peaks is increased and in particular, those observed at  $132, 287, 336, 355, 410$  and  $671 \text{ cm}^{-1}$ . The peaks shift to the left with the appearance of a new peak at around  $208 \text{ cm}^{-1}$ . The sample with rapid cooling presents a disordered kesterite structure (I-42m) and the sample with slow cooling has a

weakly disordered structure. However, the peak observed at  $336\text{ cm}^{-1}$  remains the main peak.

The addition of Si to the structure shifts the peaks towards high values of the wavenumber (Figure 3); for example, the most intense peak evolves from  $337\text{ cm}^{-1}$  (Si00) to  $343\text{ cm}^{-1}$  for Si50 sample.

In order to quantitatively monitor the effect of silicon insertion on the position on the positions and intensity of the peaks, the deconvolution of Raman spectra was carried out using LabSpec5 software. Figure 4(a) & Figure 4(b) shows the deconvolution of Raman spectra of Si00-21 and Si50-A1 samples. A displacement of the majority peaks of Si00-21 sample from  $255, 286, 337, 352, 373, 410, 610$  et  $669\text{ cm}^{-1}$  to  $271, 294, 343, 358, 370, 415, 623$  et  $687\text{ cm}^{-1}$  when 50% Sn is replaced by 50%Si (Si50-A1). However, some peaks remain in the same position ( $147$  and  $314\text{ cm}^{-1}$ ) and the addition of silicon has no effect on the peak positions. Moreover, some peaks ( $471$  and  $581\text{ cm}^{-1}$ ) exist only in sample without Sn. The evolution of the position of the intense peak as a function of Si content for the tetragonal solid solution ( $0 \leq x \leq 0.5$ ) is shown in Figure 5, and confirms the shift of this peak to high value with the increase of Si content.

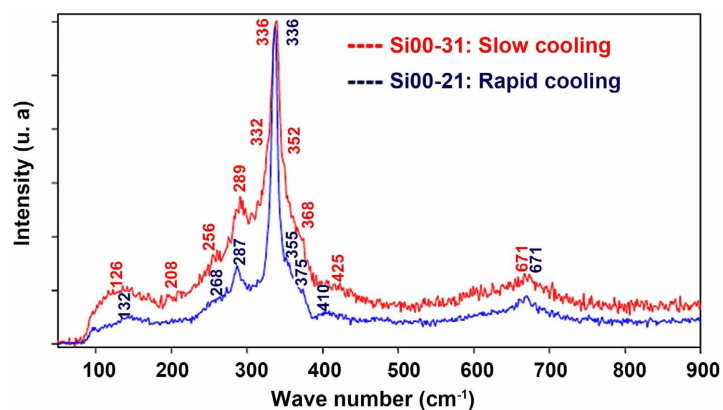


Figure 2. Raman spectra of compounds Si00-21 (rapid cooling) and Si00-31 (slow cooling).

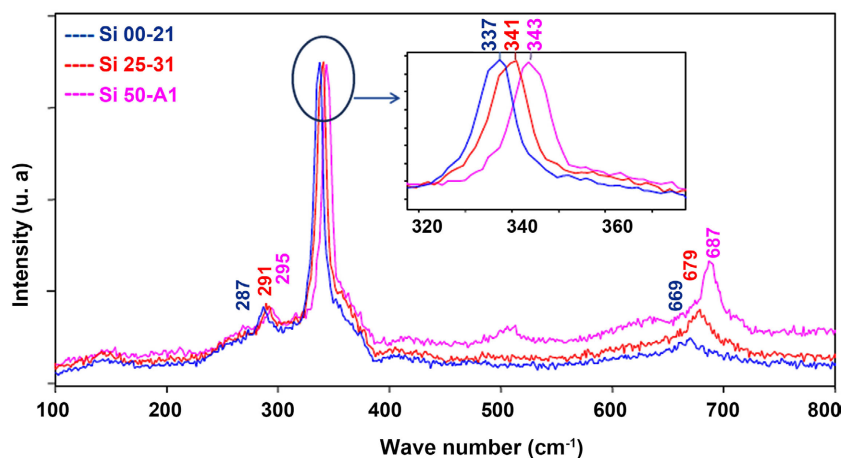
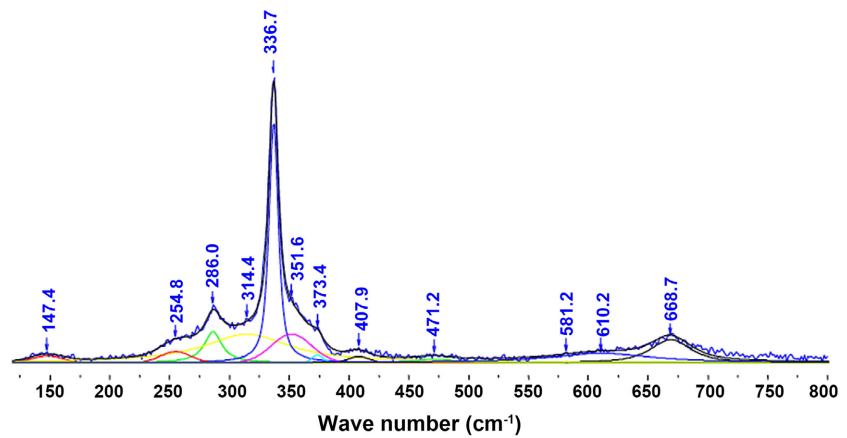
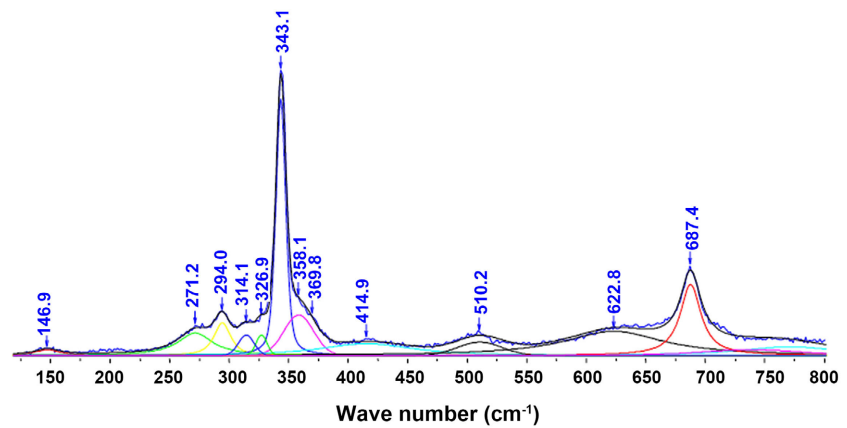


Figure 3. Raman spectra of compounds at different silicon compositions.



(a)



(b)

**Figure 4.** (a). Raman spectrum deconvolution recorded with a wavelength of 514 nm of Si00-21 sample. (b). Raman spectrum deconvolution recorded with a wavelength of 514 nm of Si50-A1 sample.

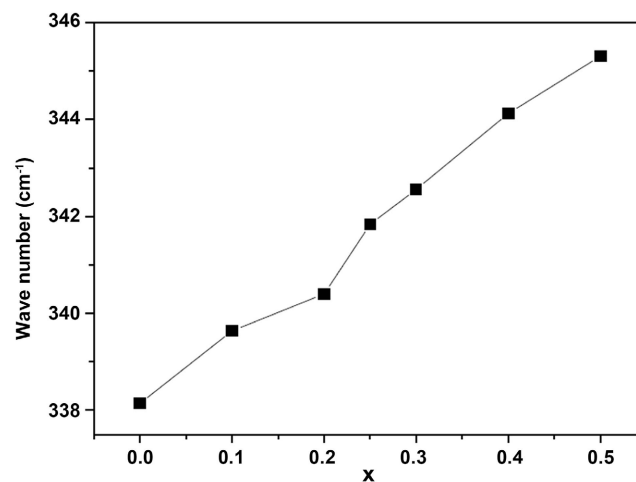
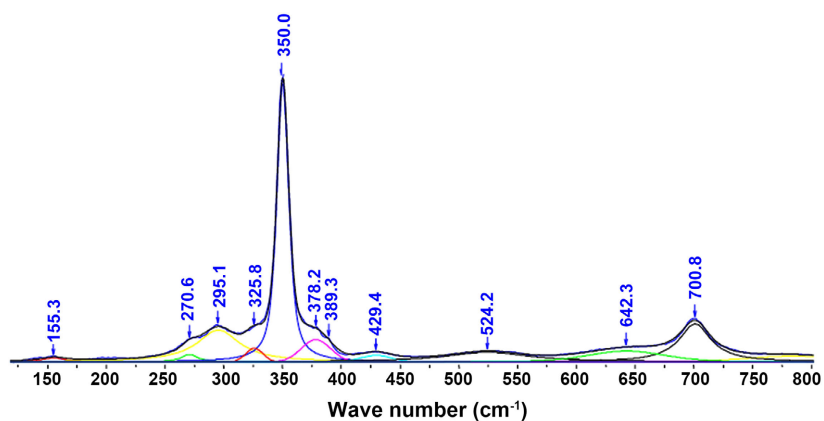


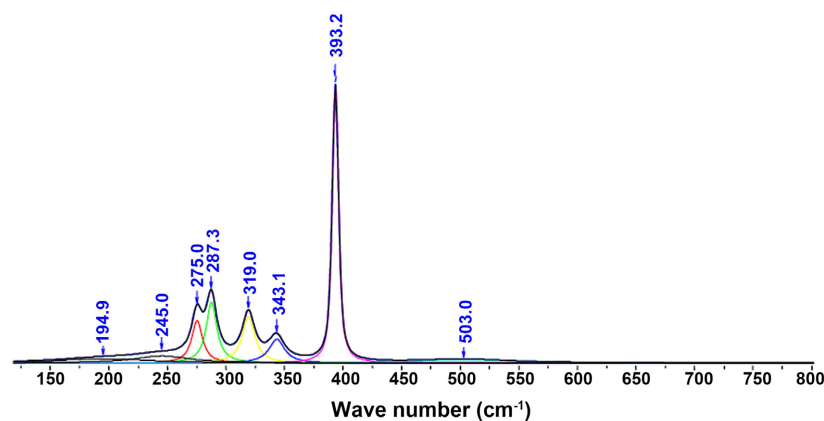
**Figure 5.** Evolution of the position of the intense peak as a function of x.

However, the deconvolution of Raman spectra of orthorhombic solid solution ( $x \geq 0.8$ ) presented in **Figure 6** reveals that the intense peak of the sample with

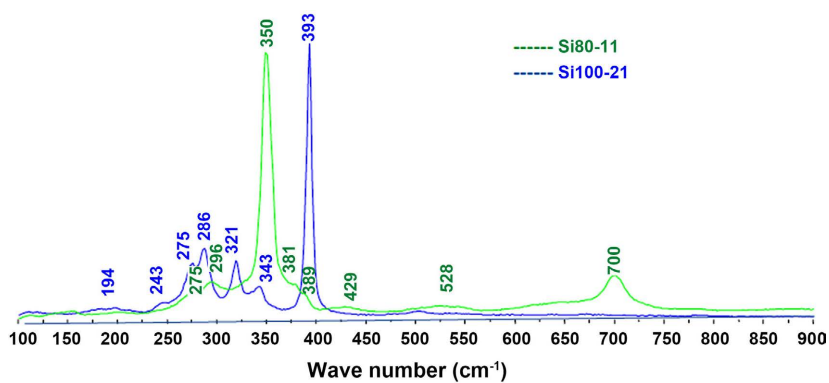
80% of Si appears at  $350\text{ cm}^{-1}$  while that of  $x = 1$  appears at  $393\text{ cm}^{-1}$ . As observed in tetragonal solid solution, new peaks appear only in the sample without Sn content (194, 243 and  $393\text{ cm}^{-1}$ ) and also in the sample with Sn content, 831, 429, 528 and  $700\text{ cm}^{-1}$  (Figure 6(c)). All peaks obtained in Raman spectrum of the sample without Sn (Si100-21) are similar and in accordance to those found in the literature [31].



(a)



(b)



(c)

**Figure 6.** (a). Raman spectrum deconvolution of Si80-11 sample. (b). Raman spectrum deconvolution of Si100-21 sample. (c). Superposition of the two Raman spectra (Si80-11 and Si100-21) of the orthorhombic solid solution.

### 3.3. Nuclear Magnetic Resonance (NMR)

Among the various spectroscopic methods used to access to the microscopic information about the local structures, NMR of solid is regarded as one of the most important. Magic Angle Spinning (MAS) technique is commonly used to explore polycrystalline powders. In this study, the close range chemical environments of our synthesized compounds were studied by using the solid state  $^{119}\text{Sn}$ ,  $^{65}\text{Cu}$  and  $^{29}\text{Si}$  MAS NMR spectroscopy. The chemical shift of the Sn isotope ( $^{119}\text{Sn}$ ) with the spin of 1/2 is very sensitive to its chemical surrounding; the atoms located beyond the first coordination sphere have an observable impact on the chemical shift interaction.

In the ordered kesterite structure of CZTS compound, the all Sn atoms occupy the same crystallographic site and have strictly the same environment with 4 S atoms having as environment: Cu (2a), Sn (2b), Cu (2c), Zn (2d). They must all produce an NMR signal with the same chemical shift, which must consist of a fine single and symmetrical signal located at  $-122$  ppm in agreement with the reported values for kesterite structure [32].  $^{119}\text{Sn}$  MAS NMR spectra for different content of Si are displayed in **Figure 7(a)**.

The insertion of Si in the structure reveals certain criteria. Firstly, the chemical shift increases gradually with the increase of Si content. Secondly, the lines widen remarkably from  $x \geq 0.1$  which can be attributed to the insertion effect of Si in the structure.  $^{119}\text{Sn}$  MAS NMR spectra show the presence of Sn/Si disorder as a function of the Si content in the structure, this disorder is originate from the difference in atomic radii between Sn and Si occupying the same crystallographic site. The disorder is more pronounced in the case of samples with orthorhombic structure.

It should be noted that the quadrupole interaction is sensitive to the site geometry which is described by two parameters, the quadrupolar constant ( $C_Q$ ) and the asymmetry ( $\eta_Q$ ), where  $Q$  is the electric quadrupole moment. In the CZTS kesterite structure, all copper and zinc atoms occupy tetrahedral sites formed by four sulfur atoms. The more these tetrahedral are distorted, the higher the value of  $C_Q$ . However, the copper atoms are distributed in equal quantity on two distinct sites (Cu\_2a et Cu\_2c), which explains the presence of two lines on the  $^{65}\text{Cu}$  MAS NMR spectrum (**Figure 7(b)**).

According to a Choubrac *et al.* [32] [33] [34], the Cu/Zn disorder in  $\text{Cu}_2\text{ZnSnS}_4$  compound is most important with sample rapidly cooled than that of sample slowly cooled sample. The  $^{65}\text{Cu}$  MAS NMR spectrum with wide and distorted band is observed (**Figure 7(b)**). Nevertheless, the substitution of Sn by Si brings another Si/Sn structural disorder.

The  $^{65}\text{Cu}$  MAS NMR spectra of the quadratic solid solution ( $0 \leq x \leq 0.5$ ) confirm the presence of the two copper sites (Cu-2a and Cu-2c) at 780 ppm for the samples with  $x < 0.3$  [32]. For  $x \geq 0.3$ , the insertion of Si in the structure modifies the Cu environment with wider band which explains the presence of a distribution of chemical shifts and gradient of electric fields. It is concluded that the Sn/Si disorder is much greater than that provided by Cu/Zn.

While in the case of the orthorhombic solid solution samples ( $0.8 \leq x \leq 1$ ), we observed the presence of a very broad band compared to that observed for quadratic solid solution.  $\text{Cu}_2\text{ZnSiS}_4$  sample ( $x = 1$ ) present two peaks which may be to the presence of impurities and/or to the environment around the copper atoms (**Figure 7(c)**).

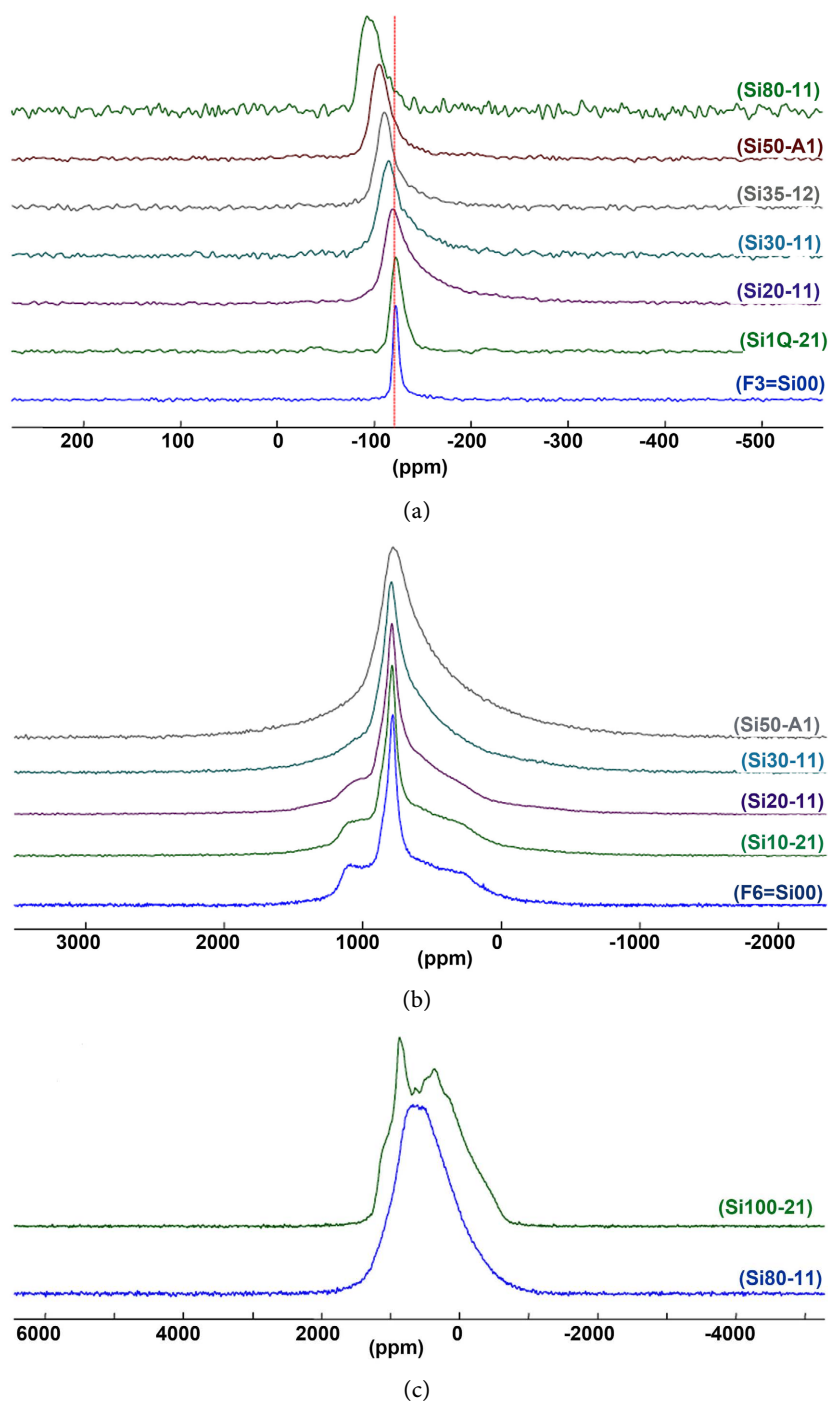


**Figure 7.** (a).  $^{119}\text{Sn}$  NMR spectra at different compositions. (b).  $^{65}\text{Cu}$  NMR spectra at different compositions of the tetragonal solid solution. (c).  $^{65}\text{Cu}$  NMR spectra at different compositions of the orthorhombic solid solution.

The  $^{29}\text{Si}$  MAS NMR spectrum which has  $1/2$  as spin is shown in **Figure 8**. The  $\text{Cu}_2\text{ZnSiS}_4$  sample indicates the presence of one band at  $-4.4$  ppm. For  $x = 0.8$  (Si80-11), an enlargement of the band is observed which is due probably to the new environment with the presence of the structural disorder Sn/Si. However, for quadratic solid solution two peaks are observed and the intensity of each peak is not regular. For low content of Si (Si25-31), the left peak is more intense while for the other samples with more Si content (Si35-11 and Si50-A1) the right one is more intense. Thus can be attributed to the insertion effect of Si in the structure and to the two very close silicon sites (Si-S4).

### 3.4. Optical Properties

The optical gap values ( $E_g$ ) of the as-prepared  $\text{Cu}_2\text{ZnSn}_{1-x}\text{Si}_x\text{S}_4$  ( $0 \leq x \leq 1$ ) are determined from the measurement of the UV-Vis diffuse reflectance spectra. The band gap can be determined by extrapolation to the energy axis of the linear plots of  $(1 - R)^2/2R$  as a function of the photon energy ( $E$  (eV)).

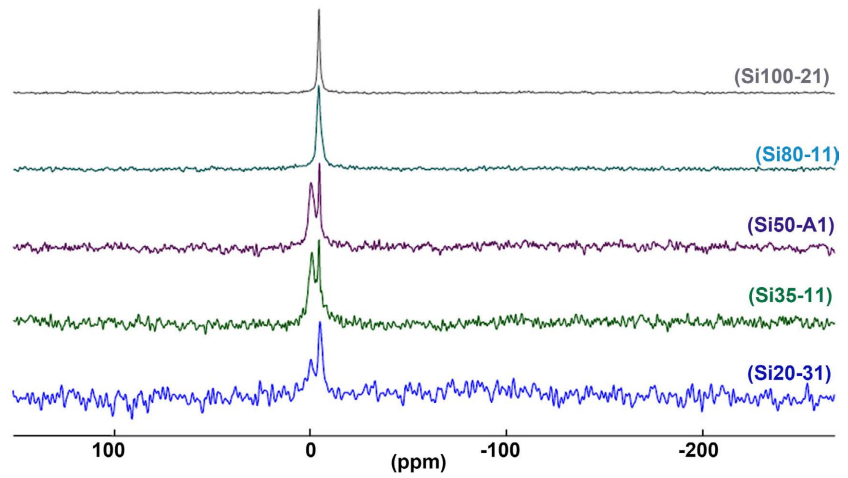
**Figure 9(a)** illustrates the UV-Vis diffused reflectance spectra obtained for the quadratic solid solution. The optical band gap energies ( $E_g$ ) for the as-prepared  $\text{Cu}_2\text{ZnSn}_{1-x}\text{Si}_x\text{S}_4$  compounds confirm a semiconductors character, and the band gap values increase from 1.38 to 2.08 eV with the increase of Si content [25] [35] [36]. For  $0.5 < x < 0.8$  (**Figure 9(b)**), UV-Vis diffused reflectance spectra reveal the presence of two different linear regions in according with the presence of two phases. The optical band gap values are 1.75 and 1.78 eV for Si60-11 and Si75-11 samples, respectively. These values are closed to those obtained for quadratic solid solution. The  $E_g$  values of the second region are 2.35 and 2.43 eV in accordance with  $E_g$  values reported in the literature for orthorhombic solid solution [37].

For  $x \geq 0.8$ , the samples present orthorhombic (wurtzite-derived) structure and the optical band gap values are 2.08 and 2.6 eV for  $x = 0.8$  and  $x = 1.0$ , respectively (**Figure 9(c)**). The  $E_g$  value of  $\text{Cu}_2\text{ZnSiS}_4$  ( $x = 1.0$ ) is closed to that found in the literature [38] [39]. In summary, the band gap values increase with the substitution of tin by silicon and rise from 1.31 eV for  $\text{Cu}_2\text{ZnSnS}_4$  ( $x = 0$ ) to 2.6 eV for  $\text{Cu}_2\text{ZnSiS}_4$  ( $x = 1$ ).

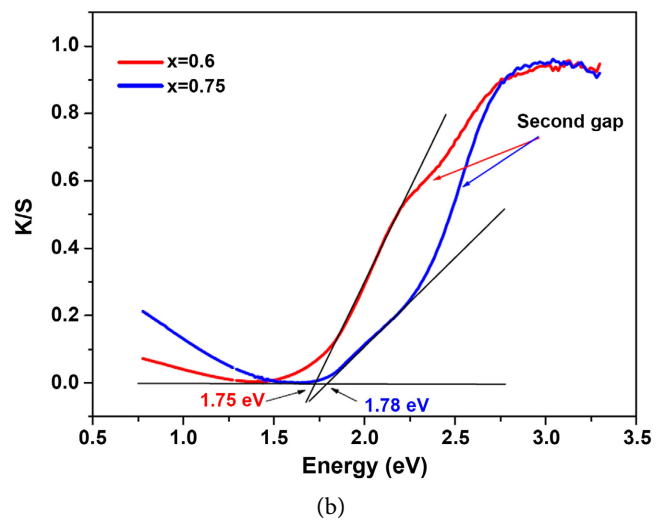
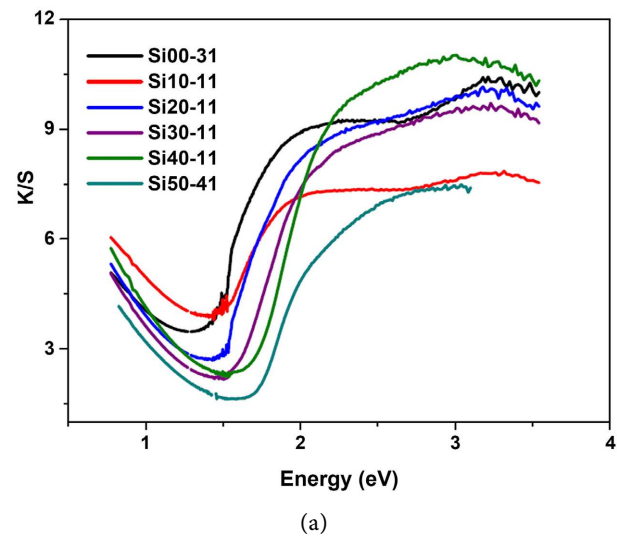
In addition to the composition of the sample which influences the band gap, the grain size can be an interesting parameter to monitor the band gap value. Si50-31 sample was used to study the effect of the different milling modes on the  $E_g$  value. **Figure 10** shows the obtained UV-Vis diffused reflectance spectra of  $\text{Cu}_2\text{ZnSn}_{0.5}\text{Si}_{0.5}\text{S}_4$  using hand grinding in a mortar and ball milling in a planetary crusher for 15 and 180 min.

The milling parameters have a considerable impact on the final value of  $E_g$ . Hand grinding and ball milling for 15 min allows to obtain very close value of  $E_g$ , 1.74 and 1.72 eV, respectively (**Figure 11**). However, the planetary milling for 180 min decrease the band gap value to 1.48 eV which can be attributed to the fine grain microstructure obtained by ball milling process and confirmed by the

XRD patterns. The peaks of the XRD pattern of the powder ball milled for 180 min are wide compared to that obtained for 15 min.



**Figure 8.**  $^{29}\text{Si}$  NMR spectra at different rapidly cooled silicon compositions.



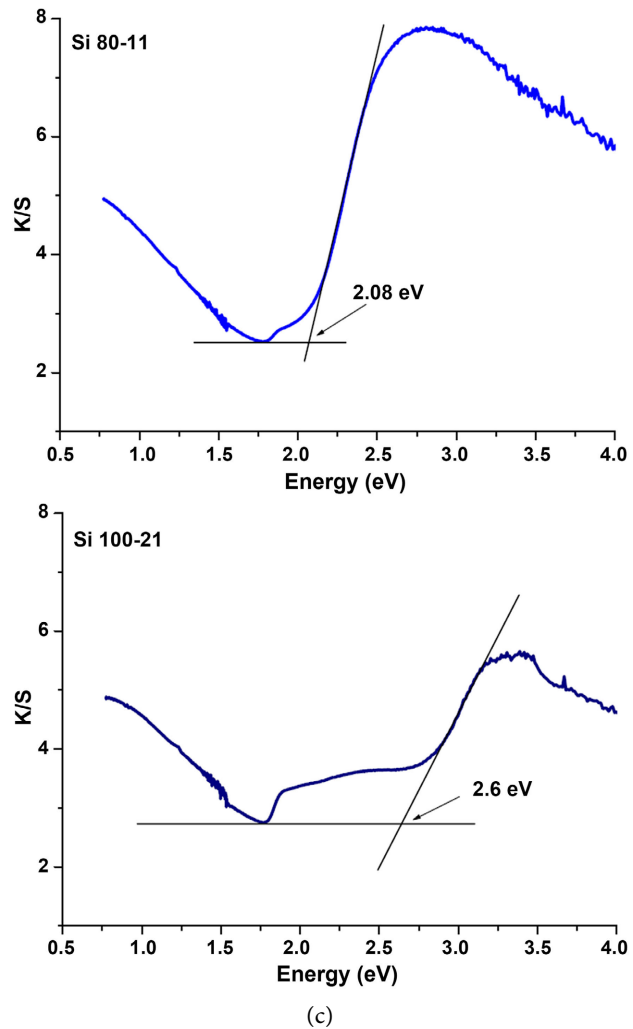


**Figure 9.** (a). Diffuse reflectance spectra of compounds of the quadratic solid solution. (b). The diffuse reflectance spectra of the compounds Si60-11 and Si75-11 or the presence of two gaps. (c). Diffuse reflectance spectra of compounds in the orthorhombic solid solution.

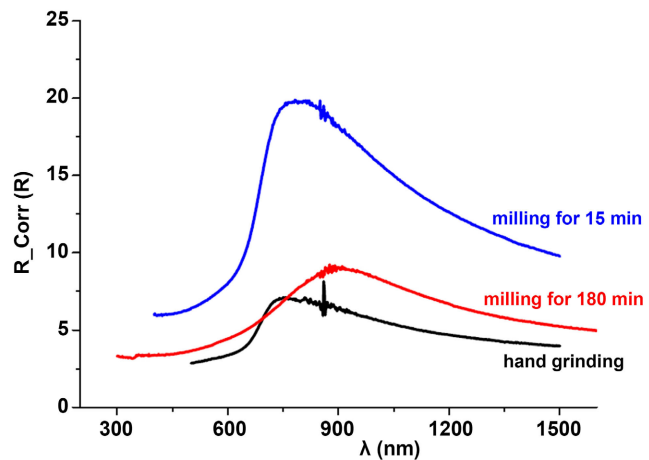


**Figure 10.** Diffuse reflectance spectra as a function of the wavelength of the Si50-31 sample (grinding effect).

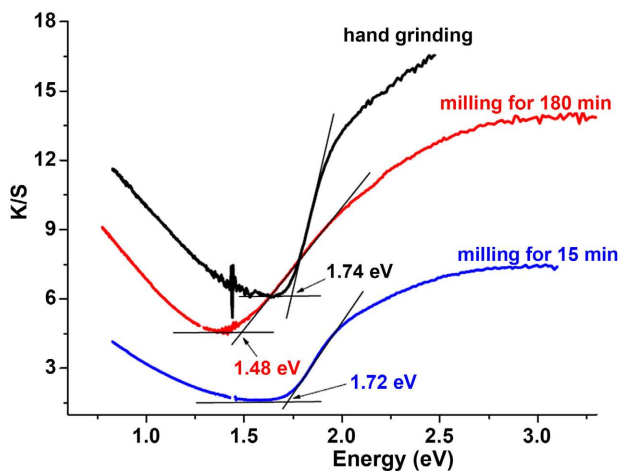


**Figure 11.** K/S spectra as a function of the energy of the Si50-31 sample (grinding effect).

#### 4. Conclusion

In summary,  $\text{Cu}_2\text{ZnSn}_{1-x}\text{Si}_x\text{S}_4$  ( $0 \leq x \leq 1$ ) compounds were prepared using the solid state reaction method. For low content of Si ( $x \leq 0.5$ ), the material conserved its pure tetragonal phase, and the associated lattice parameters decrease with the increase of Si content which can be attributed to the low atomic radii of Si compared to Sn. The evolution of the lattice parameters as a function of the Si content indicates a linear fit and follows Vegard's law. At high content of Si ( $0.5 < x < 0.8$ ), mixed tetragonal and orthorhombic phases were observed; followed by a pure orthorhombic phase for  $x \geq 0.8$ . Solid state MAS NMR spectroscopy was used to investigate the cationic disorder.  $^{119}\text{Sn}$  MAS NMR spectra show the presence of Sn/Si high disorder as a function of the Si content. The  $^{29}\text{Si}$  MAS NMR spectrum of  $\text{Cu}_2\text{ZnSiS}_4$  indicates the presence of one band at  $-4.4$  ppm which becomes wider for  $x = 0.8$  due to the structural disorder Sn/Si. However, for quadratic solid solution with low content of Si, two peaks are observed. The optical band gap values increase from 1.31 eV for  $\text{Cu}_2\text{ZnSnS}_4$  ( $x = 0$ ) to 2.43 eV for  $\text{Cu}_2\text{ZnSiS}_4$  ( $x = 1$ ) confirming a semiconductor character of the as-prepared compounds.

#### Acknowledgements

The author gratefully acknowledges the approval and the support of this research study by the grant no. SAT-2018-3-9-F-7691 from the Deanship of Scientific Research at Northern Border University, Arar, K.S.A.

#### Conflicts of Interest

The authors declare no conflicts of interest regarding the publication of this paper.

#### References

- [1] Yuan, S.J., Wang, X.S., Zhao, Y.H., Chang, Q.Q., Xu, Z., Kong, J. and Wu, S.X.

- (2020) Solution Processed Cu(In,Ga)(S,Se)<sub>2</sub> Solar Cells with 15.25% Efficiency by Surface Sulfurization. *ACS Applied Energy Materials*, **3**, 6785-6792. <https://doi.org/10.1021/acsaem.0c00917>
- [2] Syafiq, U., Ataollahi, N., Di Maggio, R. and Scardi, P. (2019) Solution-Based Synthesis and Characterization of Cu<sub>2</sub>ZnSnS<sub>4</sub> (CZTS) Thin Films. *Molecules*, **24**, Article No. 3454. <https://doi.org/10.3390/molecules24193454>
- [3] Hadke, S.H., Levchenko, S., Lie, S., Hages, C.J., Márquez, J.A., Unold, T. and Wong, L.H. (2018) Synergistic Effects of Double Cation Substitution in Solution-Processed CZTS Solar Cells with over 10% Efficiency. *Advanced Energy Materials*, **8**, Article ID: 1802540. <https://doi.org/10.1002/aenm.201802540>
- [4] Muslih, E.Y. and Kim, K.H. (2015) Characteristics of Cu<sub>2</sub>ZnSnS<sub>4</sub> Thin Film Prepared by Calcination and Sulfurizing of Metal (Cu,Zn,Sn)-Ethanamine Precursor Complexed from Metal (Cu,Zn,Sn)-Hydrate. *Chalcogenide Letters*, **12**, 349-355.
- [5] Kapusta, K., Drygas, M., Janik, J.F., Jelen, P., Bucko, M.M. and Olejniczak, Z. (2019) From Magnetic Cubic Pre-Kesterite to Semiconducting Tetragonal Kesterite Cu<sub>2</sub>ZnSnS<sub>4</sub> Nanopowders via the Mechanochemically Assisted Route. *Journal of Alloys and Compounds*, **770**, 981-988. <https://doi.org/10.1016/j.jallcom.2018.08.135>
- [6] Safdar, A., Islam, M., Akram, M.A., Mujahid, M., Khalid, Y. and Shah, S.I. (2016) Reaction Time and Film Thickness Effects on Phase Formation and Optical Properties of Solution Processed Cu<sub>2</sub>ZnSnS<sub>4</sub> Thin Films. *Journal of Materials Engineering and Performance*, **25**, 457-465. <https://doi.org/10.1007/s11665-015-1874-6>
- [7] Swami, S.K., Kumar, A. and Dutta, V. (2013) Deposition of Kesterite Cu<sub>2</sub>ZnSnS<sub>4</sub> (CZTS) Thin Films by Spin Coating Technique for Solar Cell Application. *Energy Procedia*, **33**, 198-202. <https://doi.org/10.1016/j.egypro.2013.05.058>
- [8] Shockley, W. and Queisser, H.J. (2004) Detailed Balance Limit of Efficiency of *p-n* Junction Solar Cells. *Journal of Applied Physics*, **32**, 510-519. <https://doi.org/10.1063/1.1736034>
- [9] Fernandes, P., Salomé, P.M.P. and da Cunha, A.F. (2011) Study of Polycrystalline Cu<sub>2</sub>ZnSnS<sub>4</sub> Films by Raman Scattering. *Journal of Alloys and Compounds*, **509**, 7600-7606. <https://doi.org/10.1016/j.jallcom.2011.04.097>
- [10] Wang, J.S., Li, S., Cai, J.J., Shen, B., Ren, Y.P. and Qin, G.W. (2013) Cu<sub>2</sub>ZnSnS<sub>4</sub> Thin Films: Facile and Cost-Effective Preparation by RF-Magnetron Sputtering and Texture Control. *Journal of Alloys and Compounds*, **552**, 418-422. <https://doi.org/10.1016/j.jallcom.2012.11.082>
- [11] Malerba, C., Biccari, F., Ricardo, C.L.A., Valentini, M., Chierchia, R., Müller, M., Santoni, A., Esposito, E., Mangiapane, P., Scardi, P. and Mittiga, A. (2014) CZTS Stoichiometry Effects on the Band Gap Energy. *Journal of Alloys and Compounds*, **582**, 528-534. <https://doi.org/10.1016/j.jallcom.2013.07.199>
- [12] Zhou, F.Z., Zeng, F.Q., Liu, X., Liu, F.Y., Song, N., Yan, C., *et al.* (2015) Improvement of *J<sub>sc</sub>* in a Cu<sub>2</sub>ZnSnS<sub>4</sub> Solar Cell by Using a Thin Carbon Intermediate Layer at the Cu<sub>2</sub>ZnSnS<sub>4</sub>/Mo Interface. *ACS Applied Materials & Interfaces*, **7**, 22868-22873. <https://doi.org/10.1021/acsaami.5b05652>
- [13] Litvinchuk, A.P., Dzhagan, V.M., Yukhymchuk, V.O., Valakh, M.Y., Parasyuk, O.V., Piskach, L.V., *et al.* (2016) Crystal Structure and Vibrational Properties of Cu<sub>2</sub>ZnSiSe<sub>4</sub> Quaternary Semiconductor. *Physica Status Solidi (B)*, **253**, 1808-1815. <https://doi.org/10.1002/pssb.201600175>
- [14] Kevin, P., Malik, M.A., McAdams, S. and O'Brien, P. (2015) Synthesis of Nanoparticulate Alloys of the Composition Cu<sub>2</sub>Zn<sub>1-x</sub>Fe<sub>x</sub>SnS<sub>4</sub>: Structural, Optical, and Magnetic Properties. *Journal of the American Chemical Society*, **137**, 15085-15089.

- <https://doi.org/10.1021/jacs.5b10281>
- [15] Gershon, T., Lee, Y.S., Antunez, P. Mankad, R., Singh, S., Bishop, D., *et al.* (2016) Photovoltaic Materials and Devices Based on the Alloyed Kesterite Absorber ( $\text{Ag}_x\text{Cu}_{1-x}\text{ZnSnSe}_4$ ). *Advanced Energy Materials*, **6**, Article ID: 1502468. <https://doi.org/10.1002/aenm.201502468>
- [16] Berg, D.M., Arasimowicz, M., Djemour, R., Gütay, L., Siebentritt, S., Schorr, S., *et al.* (2014) Discrimination and Detection Limits of Secondary Phases in  $\text{Cu}_2\text{ZnSnS}_4$  Using X-Ray Diffraction and Raman Spectroscopy. *Thin Solid Films*, **569**, 113-123. <https://doi.org/10.1016/j.tsf.2014.08.028>
- [17] Tanaka, T., Nagatomo, T., Kawasaki, D., Nishio, M., Guo, Q., Wakahara, A., Yoshida, A. and Ogawa, H. (2005) Preparation of  $\text{Cu}_2\text{ZnSnS}_4$  Thin Films by Hybrid Sputtering. *Journal of Physics and Chemistry of Solids*, **66**, 1978-1981. <https://doi.org/10.1016/j.jpics.2005.09.037>
- [18] Nitsche, R., Sargent, D.F. and Wild, P. (1967) Crystal Growth of Quaternary  $\text{Zn}_2\text{S}_4$  Chalcogenides by Iodine Vapor Transport. *Journal of Crystal Growth*, **1**, 52-53. [https://doi.org/10.1016/0022-0248\(67\)90009-7](https://doi.org/10.1016/0022-0248(67)90009-7)
- [19] Tombak, A., Ocak, Y.S., Genişel, M.F. and Kilicoglu, T. (2014) Electrical and Optical Properties of  $\text{Cu}_2\text{ZnSnS}_4$  Grown by a Thermal Co-Evaporation Method and Its Diode Application. *Materials Science in Semiconductor Processing*, **28**, 98-102. <https://doi.org/10.1016/j.mssp.2014.07.006>
- [20] Thimsen, E., Riha, S.C., Baryshev, S.V., Martinson, A.B.F., Elam, J.W. and Pellin, M.J. (2012) Atomic Layer Deposition of the Quaternary Chalcogenide  $\text{Cu}_2\text{ZnSnS}_4$ . *Chemistry of Materials*, **24**, 3188-3196. <https://doi.org/10.1021/cm3015463>
- [21] Ali, A., Jacob, J., Ashfaq, A., Tamseel, M., Mahmood, K., Amin, N., Hussain, S., Ahmad, W., Rehman, U. and Ikram, S. (2019) Modulation of Structural, Optical and Thermoelectric Properties of Sol-Gel Grown CZTS Thin Films by Controlling the Concentration of Zinc. *Ceramics International*, **45**, 12820-12824. <https://doi.org/10.1016/j.ceramint.2019.03.202>
- [22] Song, N., Green, M.A., Huang, J.L., Hu, Y.C. and Hao, X.J. (2018) Study of Sputtered  $\text{Cu}_2\text{ZnSnS}_4$  Thin Films on Si. *Applied Surface Science*, **459**, 700-706. <https://doi.org/10.1016/j.apsusc.2018.07.192>
- [23] Patel, S.B. and Gohel, J. V. (2018) Enhanced Solar Cell Performance by Optimization of Spray Coated CZTS Thin Film Using Taguchi and Response Surface Method. *Journal of Materials Science: Materials in Electronics*, **29**, 5613-5623. <https://doi.org/10.1007/s10854-018-8530-5>
- [24] Choubrac, L., Lafond, A., Guillot-Deudon, C., Moëlo, Y. and Jobic, S. (2012) Structure Flexibility of the  $\text{Cu}_2\text{ZnSnS}_4$  Absorber in Low-Cost Photovoltaic Cells: From the Stoichiometric to the Copper-Poor Compounds. *Inorganic Chemistry*, **51**, 3346-3348. <https://doi.org/10.1021/ic202569q>
- [25] Hamdi, M., Lafond, A., Guillot-Deudon, C., Hlel, F., Gargouri, M. and Jobic, S. (2014) Crystal Chemistry and Optical Investigations of the  $\text{Cu}_2\text{Zn}(\text{Sn},\text{Si})\text{S}_4$  Series for Photovoltaic Applications. *Journal of Solid State Chemistry*, **220**, 232-237. <https://doi.org/10.1016/j.jssc.2014.08.030>
- [26] Fournet, G. (1953) Étude de la loi de Vegard. *Journal de Physique et le Radium*, **14**, 374-380.
- [27] Rosmus, K.A. and Aitken, J.A. (2011)  $\text{Cu}_2\text{ZnSiS}_4$ . *Acta Crystallographica Section E*, **67**, i28. <https://doi.org/10.1107/S1600536811008889>
- [28] Khare, A., Himmetoglu, B., Cococcioni, M. and Aydil, E.S. (2012) First Principles

- Calculation of the Electronic Properties and Lattice Dynamics of  $\text{Cu}_2\text{ZnSn}(\text{S}_{1-x}\text{Se}_x)_4$ . *Journal of Applied Physics*, **111**, Article ID: 123704. <https://doi.org/10.1063/1.4728232>
- [29] Gurel, T., Sevik, C. and Cagin, T. (2011) Characterization of Vibrational and Mechanical Properties of Quaternary Compounds  $\text{Cu}_2\text{ZnSnS}_4$  and  $\text{Cu}_2\text{ZnSnSe}_4$  in Kesterite and Stannite Structures. *Physical Review B*, **84**, Article ID: 205201. <https://doi.org/10.1103/PhysRevB.84.205201>
- [30] Caballero, R., Garcia-Llamas, E., Merino, J.M., León, M., Babichuk, I., Dzhegagan, V., Strelchuk, V. and Valakh, M. (2014) Non-Stoichiometry Effect and Disorder in  $\text{Cu}_2\text{ZnSnS}_4$  Thin Films Obtained by Flash Evaporation: Raman Scattering Investigation. *Acta Materialia*, **65**, 412-417. <https://doi.org/10.1016/j.actamat.2013.11.010>
- [31] Guc, M., Levchenko, S., Izquierdo-Roca, V., Fontane, X., Valakh, M., Arushanov, E. and Pérez-Rodríguez, A. (2013) Polarized Raman Scattering Analysis of  $\text{Cu}_2\text{ZnSnSe}_4$  and  $\text{Cu}_2\text{ZnGeSe}_4$  Single Crystals. *Journal of Applied Physics*, **114**, Article ID: 193514.
- [32] Choubrac, L., Paris, M., Lafond, A., Guillot-Deudon, C., Rocquefelte X. and Jobic, S. (2013) Multinuclear ( $^{67}\text{Zn}$ ,  $^{119}\text{Sn}$  and  $^{65}\text{Cu}$ ) NMR Spectroscopy—An Ideal Technique to Probe the Cationic Ordering in  $\text{Cu}_2\text{ZnSnS}_4$  Photovoltaic Materials. *Physical Chemistry Chemical Physics*, **15**, 10722-10725. <https://doi.org/10.1039/c3cp51320c>
- [33] Nicole, J., Elizabeth, P. and Angus, R. (2016) Multi-Nuclear ( $^{119}\text{Sn}$  and  $^{65}\text{Cu}$ ) NMR and Raman Spectroscopy to Probe Secondary Phases in  $\text{Cu}_2\text{ZnSnS}_4$ . 2016 *IEEE 43rd Photovoltaic Specialists Conference (PVSC)*, Portland, 5-10 June 2016, 3046-3050. <https://doi.org/10.1109/PVSC.2016.7750224>
- [34] Elizabeth, A.P., Andre, S., Nicole, E.J., Daniel, P.S. and Angus, A.R. (2017) Oxygen-Induced Ordering in Bulk Polycrystalline  $\text{Cu}_2\text{ZnSnS}_4$  by Sn Removal. *Inorganic Chemistry*, **56**, 12328-12336. <https://doi.org/10.1021/acs.inorgchem.7b01777>
- [35] Kahraman, S., Cetinkaya, S., Cetinkara, H.A. and Guder, H.A. (2014) Effects of Diethanolamine on Sol-Gel-Processed  $\text{Cu}_2\text{ZnSnS}_4$  Photovoltaic Absorber Thin Films. *Materials Research Bulletin*, **50**, 165-171. <https://doi.org/10.1016/j.materresbull.2013.10.043>
- [36] Guc, M., Levchenko, S., Dermenji, L., Gurieva, G., Schorr, S., Syrbu, N.N. and Arushanov, E. (2014) Excitation Spectra and Energy Band Structure of  $\text{Cu}_2\text{ZnSiSe}$ . *Journal of Alloys and Compounds*, **587**, 393-397. <https://doi.org/10.1016/j.jallcom.2013.10.172>
- [37] Levchenko, S., Dumcenco, D., Huang, Y.S., Arushanov, E., Tezlevan, V., Tiong, K.K. and Du, C.H. (2011) Absorption-Edge Anisotropy of  $\text{Cu}_2\text{ZnSiQ}_4$  (Q=S, Se) Quaternary Compound Semiconductors. *Journal of Alloys and Compounds*, **509**, 4924-4928. <https://doi.org/10.1016/j.jallcom.2011.01.169>
- [38] Levchenko, S., Dumcenco, D., Huang, Y.S., Arushanov, E. and Tezlevan, V. (2010) Near Band Edge Anisotropic Optical Transitions in Wide Band Gap Semiconductor  $\text{Cu}_2\text{ZnSiS}_4$ . *Journal of Applied Physics*, **108**, Article ID: 73508.
- [39] Zamulko, S., Chen, R. and Persson, C. (2017) Investigation of the Structural, Optical and Electronic Properties of  $\text{Cu}_2\text{Zn}(\text{Sn,Si/Ge})(\text{S/Se})_4$  Alloys for Solar Cell Applications. *Physica Status Solidi (B)*, **254**, Article ID: 1700084. <https://doi.org/10.1002/pssb.201700084>